JACS Au
AN OPEN ACCESS JOURNAL OF THE AMERICAN CHEMICAL SOCIETY

Open Access
This article is licensed under CC-BY-NC-ND 4.0

pubs.acs.org/jacsau
Article

On the Importance of Configuration Search to the Predictivity of Lanthanide Selectivity

Thomas J. Summers, Michael G. Taylor, Logan J. Augustine, Jan Janssen, Danny Perez, Enrique R. Batista, and Ping Yang*

Cite This: JACS Au 2025, 5, 631−641
Read Online

ACCESS | Metrics & More | Article Recommendations | Supporting Information

ABSTRACT: The lanthanide elements are crucial components in numerous technologies, yet their industrial production through liquid−liquid extraction continues to be economically and environmentally costly due to the challenge of separating elements with similar physicochemical properties. While computational ligand screening has shown promise toward discovering efficient extractants, the complexity of constructing chemically sensible 3D structures (often by hand), coupled with the high cost of quantum chemistry calculations, often limits exploration of the vast ligand chemical and conformational space in favor of local exploration around known chemistries. Moreover, metal complexes can have many stable configurations whose differences in energies exceed the small energy differences that determine the extractant selectivity for certain lanthanides. Because of this difference, incorrect selectivity predictions can be made if the lowest energy coordination complex is not identified and modeled. To address this issue, we present a high-throughput computational workflow that automates the construction and quantum mechanical modeling of 3D lanthanide-extractant complexes. This approach allows for an unbiased search of distinct configurational and compositional variations for each metal, enabling accurate predictions of their solution structures and lanthanide selectivity. As showcased by three extractants from diverse chemical categories—a crown ether, a phenanthroline monocarboxamide, and a malonamide—it is found that sampling the lanthanide-ligand configuration space is critical to correctly predicting the metal coordination environment and experimental lanthanide selectivity trends.

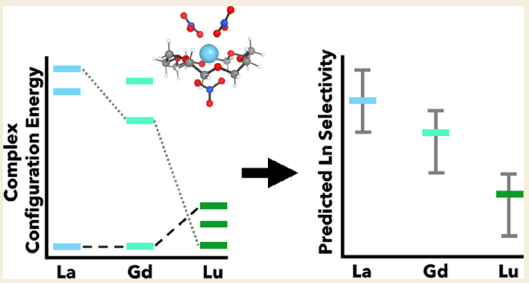

KEYWORDS: *lanthanides, solvent extraction, metal complexes, configurational sampling, metal selectivity*

INTRODUCTION

Climate change is, arguably, one of the most pressing issues facing society.[1] Many emerging technologies aimed at mitigating climate change, such as wind turbines, electric vehicles, LED lights, and batteries,[2] rely on rare earth elements, including yttrium, scandium, and the 14 lanthanide (Ln) elements. However, extracting and separating these rare earth elements from ores,[3] recycled electronics,[4] or spent nuclear fuel[5] is challenging and costly due to their similar physical and chemical properties. Currently, liquid−liquid extraction is the primary method used for separation, where extractant molecules dissolved in organic solvents selectively bind and transfer targeted aqueous Ln's into an organic phase.[6] This process is particularly difficult for separating adjacent or near-adjacent Ln's, with reported separation factors for many commercial extractants being less than 5.[7−10] As such, achieving a high purity for specific metals requires multiple extraction cycles, resulting in high reagent consumption and liquid waste generation. This process has a significant environmental footprint,[11,12] necessitating the development of either new separation processes or extractants with improved efficiency to reduce this impact.[13]

Developing novel extractants with strong selectivity for individual Ln's is challenging due to the nearly identical charge densities of Ln^{3+} ions, which give them similar physical and chemical properties.[14] Identifying ligands to synthesize and test typically relies on scientific intuition or knowledge gained from experience, which can limit the scope of extractants explored to incremental variants of previously reported structures.[15−17] A comprehensive understanding of how different ligand types affect coordination geometry, binding, and selectivity for Ln's is crucial to designing new extraction processes.[18−20] However, synthesizing, testing the extraction properties, and characterizing the binding structure for a massive set of diverse ligands are expensive and labor-intensive. To gain insights into ligand selectivity and binding without high experimental costs, theoretical modeling of Ln-ligand complexes can be utilized. Classical molecular dynamics and metadynamics simulations

Received: August 22, 2024
Revised: November 4, 2024
Accepted: November 5, 2024
Published: November 18, 2024

© 2024 The Authors. Published by American Chemical Society

https://doi.org/10.1021/jacsau.4c00770
JACS Au 2025, 5, 631−641

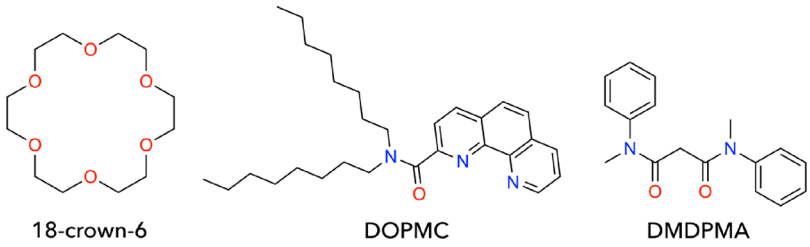

Figure 1. Three ligands explored in this work.

have proven to be powerful tools for probing Ln-extractant structure and solvation environments, but their computing requirements can limit their use for high-throughput screening of diverse ligands.[21−23] High-level quantum chemistry computations have been successfully applied to various Ln-ligand complexes, including aminopolycarboxylic acids, N-heterocycles, and dithiophosphoric acids.[24−31] Normally, the modeled structures are taken from X-ray crystal structures or by-hand designs, but this approach has limitations for exploring new ligands as (1) it requires prior knowledge of the extracted Ln complex structure and (2) it is difficult to ensure structures converge to the global thermodynamically favored configuration and not a local minimum state.[32−34]

The selectivity of extractants for different Ln's is typically dictated by differences in the physico-chemistry of their Ln-complexes on the order of only a few kcal/mol (e.g., a 1.4 kcal/mol energy difference roughly refers to a separation factor of 10 at the equilibrium).[35] However, metal−ligand complexes with multiple geometric configurations and ligand conformers can exhibit a multitude of chemically sensible, thermodynamically stable geometries, with conformer energies ranging more than 10 kcal/mol.[36−38] As such, the energetic differences from modeling these local minimum structures instead of the lowest energy structures can overshadow the chemistry that determines extractant selectivity and lead to incorrect predictions. Ensuring the unbiased exploration for the correct coordination complex for each metal identity requires the capability to rapidly construct chemically sensible structures that span the configurational space combined with an effective high-throughput workflow to manage the large number of quantum chemistry calculations that are not readily scalable on high-performance computing platforms.

To address these challenges, we use our recently developed *Architector* package to automate the exploration, construction, and preliminary screening of candidate metal−ligand structures at the semi-empirical tight binding level of theory.[39] The computational efficiency of *Architector* allows for the generation and optimization of numerous metal−ligand configurations without human biases, facilitating a thorough exploration of the potential energy landscape beyond what is feasible with manual methods. In this work, *Architector* is augmented with an automated asynchronous workflow, *pyiron*,[40] to predict the relative extraction properties of generated structures using density functional theory (DFT).

We apply the above high-throughput computational workflow to three ligands (Figure 1) as a case study: a crown ether (18-crown-6), a phenanthroline monocarboxamide (DOPMC), and a malonamide ligand (DMDPMA). These three ligands were chosen as they each are neutral ligands from diverse chemical categories covering differing configurational complexity (in both the number of extractants able to coordinate and side chain length). Additionally, experimental distribution coefficients for both early and late Ln's have been reported for each of the ligands, serving as benchmarks for validation.[41−43] Although these three ligands are not among the best-performing extractants for industrial Ln separation, their structural diversity makes them suitable for examining how configurational exploration impacts the prediction of lanthanide selectivity. Through these examples, we show that sampling the Ln-extractant configuration space is essential for accurately predicting both the metal coordination environment and the lanthanide selectivity trend. We note that the strategies presented in this work are directly translatable to other fields, such as organometallic catalysis, where the catalyst conformation is known to impact simulated properties.

COMPUTATIONAL METHODS

Prediction of Lanthanide Selectivity

Liquid−liquid extraction involves an intricate system of competing equilibrium reactions among aqueous, organic, and interfacial phases.[35,44] The efficiency of the process is quantified by the distribution ratio (D), defined as the ratio of the final Ln concentration in the organic phase vs the aqueous phase:

$$D_{\mathrm{Ln}} = \frac{[\mathrm{Ln}]_{(\mathrm{org})}}{[\mathrm{Ln}]_{(\mathrm{aq})}} \tag{1}$$

The selectively between distinct Ln ions can be described by the ratio of their respective distribution coefficients, commonly reported as a separation factor ($\mathrm{SF}_{\mathrm{Ln1/Ln2}}$):

$$\mathrm{SF}_{\mathrm{Ln1/Ln2}} = \frac{D_{\mathrm{Ln1}}}{D_{\mathrm{Ln2}}} \tag{2}$$

Therefore, the separation factor is proportional to the ratio of the equilibrium constants for the two competing extraction reactions, which is tied to the difference in Gibbs free energies for the two equilibria as

$$\mathrm{SF}_{\mathrm{Ln1/Ln2}} = \frac{K_{\mathrm{Ln1}}}{K_{\mathrm{Ln2}}} = e^{-(\Delta G_{\mathrm{Ln1}} - \Delta G_{\mathrm{Ln2}})/RT} \tag{3}$$

To compute the theoretical difference in energies for the two equilibria, the following reaction for the competitive complexation of reference La^{3+} (Ln_2) over other Ln^{3+} (Ln_1) can be used:

$$\mathrm{La(NO_3)_3(H_2O)_{3(aq)}} + \mathrm{Ln(NO_3)_3(L)_{N(org)}} \rightleftharpoons \mathrm{Ln(NO_3)_3(H_2O)_{3(aq)}} + \mathrm{La(NO_3)_3(L)_{N(org)}} \tag{4}$$

This method leverages DFT error cancellation to help differentiate metal selectivity[35] and has been applied to multiple types of extractants.[45−48] $\Delta\Delta E_{\mathrm{La/Ln}}$ is computed here for eq 4 instead of $\Delta\Delta G_{\mathrm{La/Ln}}$ to reduce the computational cost as this difference is not expected to alter the final interpretation of predicted Ln selectivity trends. The rationale is that entropy contributions are expected to largely cancel out in the thermodynamic cycle (eq 4), which maintains similar complexes on both sides of the equation but with the metals exchanged. As validation, $\Delta\Delta G_{\mathrm{La/Ln}}$ was computed for the most stable

https://doi.org/10.1021/jacsau.4c00770
JACS Au 2025, 5, 631−641

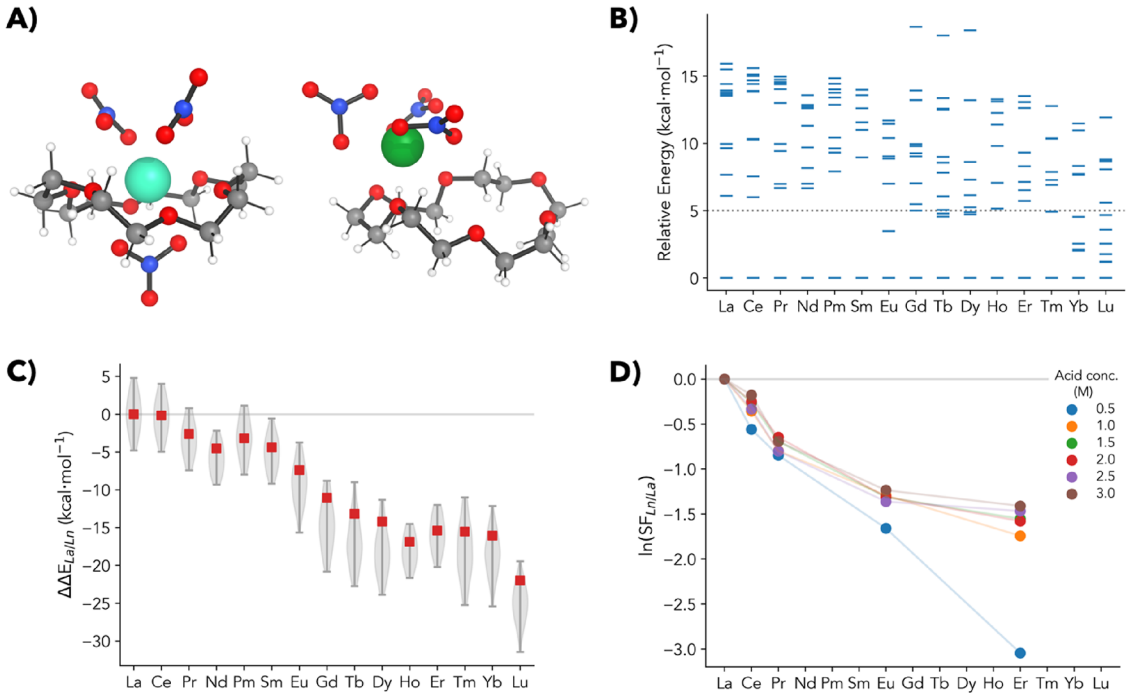

Figure 2. (A) Most stable $Ln^{III}(18\text{-crown-6})(NO_3)_3$ configuration identified for (left) Gd^{3+} and (right) Lu^{3+}. (B) Relative energies for the different configurations across the Ln's. (C) Predicted selectivity ($\Delta\Delta E_{La/Ln}$) for 18-crown-6 using the lowest energy configuration (red squares) and structures ≤5 kcal/mol of the lowest energy configuration (gray violin plots). (D) Experimental $\ln(SF_{Ln/La})$ for 100 ppm Ln^{3+} with 0.05 M 18-crown-6 in different trichloroacetic acid concentrations.[42]

La, Gd, and Lu complexes. The results showed that differences between $\Delta\Delta G_{La/Ln}$ from $\Delta\Delta E_{La/Ln}$ were typically <1 kcal/mol except for select Lu complexes where entropic differences lead to differences up to 3.5 kcal/mol but still had no meaningful impact on the selectivity trend (see Supporting Information Figure S7 for additional details).

Structure Generation and Preliminary Screening

To identify possible Ln coordination structures, *Architector* was used to construct and preliminarily screen energetically stable complexes. All complexes were created using a Gd metal center with a total coordination number ranging from 8 to 10. In total, the metal center could coordinate up to one (18-crown-6: 1,4,7,10,13,16-hexaoxacyclooctadecane), two (DOPMC: *N*,*N*-dioctyl-1,10-phenanthroline-2-carboxamide), or three (DMDPMA: *N*,*N*′-dimethyl-*N*,*N*′-diphenylmalonamide) extractant ligands, while the rest of the first shell was saturated with the addition of three nitrate ligands. The nitrate ligands primarily coordinated Gd as bidentate unless the total coordination number of the Gd exceeded 10, at which point monodentate configurations of one or more (up to three) nitrates were used. To assemble each Gd-ligand complex, up to 20 different core symmetries were constructed for each coordination number and the 10 lowest energy initial geometries (12 for 18-crown-6) were relaxed using *xTB*/GFN2-xTB.[49,50] The relative energy ranges of these stable configurations span up to 15−18 kcal/mol, an energetic difference greater than the energy contributions that direct Ln separation. To mimic the organic solution environment for the neutral Gd-ligand structures, relaxations were simulated using a toluene implicit solvent (relative permittivity ε = 2.37). Optimized structures with RMSD difference <0.4 Å were considered identical, therefore, only the lowest energy structure was kept for subsequent DFT optimization. The aqueous $Ln(NO_3)_3(H_2O)_3$ structures in eq 4 were generated using a similar process as the Ln-ligand complexes, but using water for the implicit solvation medium (ε = 78.39). See Figures S1 and S2 for additional information on the $Ln(NO_3)_3(H_2O)_3$ structures.

Density Functional Theory Calculations

The lowest energy GFN2-xTB Gd-complexes constructed by *Architector* were further optimized using DFT to identify the lowest energy structure and sample potentially thermodynamically relevant low-energy configurations. All DFT calculations were performed using the *ADF* v2022.103 software[51] with the PBE density functional, ZORA Hamiltonian[52] for relativistic effects, and Grimme's DFT-D4 correction for van der Waals interactions.[53] Additionally, an implicit solvation environment (COSMO)[54,55] was used with all organic LnL complexes modeled in toluene (ε = 2.38) and aqueous $Ln(NO_3)_3$ using water (ε = 78.39). We have previously shown that this level of theory is suitable for screening large sets of extractant structures efficiently, though more accurate energetics may require more computationally expensive methods, such as coupled-cluster level DLPNO−CCSD(T).[16] After geometry optimization, final DFT energies were calculated by performing a single point calculation with the SM12 implicit solvation model[56] (ε = 1.88 for LnL and ε = 78.39 for $Ln(NO_3)_3$) using the same level of theory described above. This was chosen as SM12 has been shown to describe the solvation energy of neutral complexes more accurately compared to COSMO.[57] Additional information about the effects of the two different solvation models is provided in Figures S4−S6. To characterize the metallo-substituted complexes and examine the selectivity trends across the Ln series, all DFT-optimized Gd complexes were replaced with the other Ln metals and subsequently reoptimized using the same workflow. All structures were initially optimized using a double-ζ basis set (DZP) with a frozen core for all atoms. These structures were further optimized using a triple-ζ basis set (TZP) with small frozen core. The comparison of the relative energies for the different configurations (Figure S3) indicated that the later lanthanides (Tb−Lu) optimize to lower coordination number structures with the TZP basis set, leading to differences in predicted relative stability. Therefore, all structures and energies reported throughout this work were calculated using the TZP basis and a small frozen core. It should be noted that even though all Ln-configuration combinations were attempted, 82 of the 810 total structures were not readily characterized due to SCF convergence failure, a known challenge

https://doi.org/10.1021/jacsau.4c00770
JACS Au 2025, 5, 631−641

for Ln complexes. Analysis of the $\langle S^2 \rangle$ showed that the final optimized structures were always within 2.6% of their value.

High-Throughput Computational Workflow

Given the complexity of this problem space for constructing and screening different Ln-extractant complex ratios, nitrate denticities, and extractant configurations at the xTB and DFT levels of theory, it is crucial to establish a high-throughput workflow capable of automating these series of computations. To effectively handle these tasks and their dependencies, calculations were managed using the open-source *pyiron* package.[40] To enable complex task management asynchronously, we built additional capabilities into the *pyiron* package leveraging the flux framework.[58] The *pyiron*/flux/*Architector* workflow is engineered for scaling and distributing batches of less-than-single compute node tasks and might have heightened latency with larger molecular system DFT evaluations, for example. Nevertheless, even with the largest systems reported in this work, this workflow enabled thousands of *Architector* runs, error checking, and subsequent DFT calculations to be performed under a single HPC allocation, resulting in a nearly 100% utilization efficiency of hundreds of nodes on a leading US DOE HPC machine. For this work, nearly 2,700 individual calculations were managed using this workflow.

RESULTS

Ln(III)-18-Crown-6

We begin by investigating the case of Ln chelated by the crown ether 18-crown-6 (Figure 1). 18-crown-6 is known to form a 1:1 complex with early to mid Ln ions, where solid-state structures show the Ln ion occupying the space within the ring, effectively in-plane with the crown ether oxygen atoms.[59−63] The trend in stability constants[64,65] for the complexes (La^{3+} > Ce^{3+} > Pr^{3+} > Nd^{3+} > Sm^{3+} > Eu^{3+} > Gd^{3+}) can be linked to the relationship between ligand cavity size and Ln ionic radii. The La^{3+} ion, with an ionic radius of 1.06 Å, fits well within the cavity (∼1.3—1.6 Å cavity size), but as ionic radii decrease across the Ln series, the ion-ring interaction weakens. This leads to little or no complex formation typically observed for the later lanthanides.

Initial screening with *Architector* led to 12 unique Gd(18-crown-6)$(NO_3)_3$ configurations, which were further optimized with DFT. Of these structures, three had the Gd^{3+} within the central ring while the nitrates were coordinated both above and below the ring plane (Figure S8). The lowest energy structure was found to have all three nitrates coordinated in a bidentate configuration (Figure 2A, coordination number CN = 12). Changing either of the bidentate nitrates to monodentate resulted in a decrease in the stability by ∼5 kcal/mol.

The remaining nine structures identified have Gd^{3+} ions located above the plane of the crown ether ring, with the ligand "wrapping" around half of the ion and the three nitrates bound to the coordination sites on the opposite half of the ion (Figure S8). Each of these structures has an energy of ≥7.3 kcal/mol from the most stable configuration for Gd^{3+}. While this alternate binding configuration for 18-crown-6 is perhaps unsurprisingly less stable than having the ion within the central cavity, this type of wrapping configuration is the preferred binding motif for macrocycles with slightly smaller cavity sizes (e.g., 15-crown-6).[61,66]

The relative energies of the Ln metallovariant configurations are shown in Figure 2B. The most stable configuration for Gd(18-crown-6) was consistently identified as the most stable configuration for the other Ln's except for Lu, whose most stable structure (by 1.16 kcal/mol) contains the ion outside the ring and coordinated to only half of the crown ether oxygens—a partially decomplexed state (Figure 2A and Figure S8). Overall, the relative energies of the alternate configurations generally decrease across the Ln series, indicating both the monodentate nitrate configurations and the wrapping crown ether structures become more stabilized as the ionic radii decrease in size. This is perhaps most starkly illustrated by how the most stable configuration for Lu is 13.66 kcal/mol higher in energy for La (Figure S9). All of these observed changes in configurational stability highlight the importance of assessing alternate structures across the series and validate the robustness of *Architector* in identifying diverse yet chemically sensible structures. Without prior experimental structure knowledge or rigorous testing, any of these models could be used for calculating Ln selectivity without obvious concerns, potentially leading to incorrect predictions of separation trends.

Figure 2C shows the competitive complexation of La^{3+} over Ln^{3+} for the most stable structures calculated using eq 4. It is observed that the computed $\Delta\Delta E_{La/Ln}$ becomes progressively more negative when going from La to Lu, indicating preferential extraction of La and the lighter Ln's into the organic phase over heavier Ln's. Previously reported[42] experimental separation factors for 18-crown-6 are plotted in Figure 2D as $\ln(SF_{Ln/La})$, where a similar trend is shown with $\ln(SF_{Ln/La})$ becoming progressively more negative across the series. Since SF is sensitive to the experimental conditions (temperature, diluent, salt, pH, contact time, extractant and metal concentrations)[67] we include all reported experimental SF values when multiple experimental conditions were measured to help indicate the influence of solvent environment factors (features outside the scope of our first shell models) on selectivity trends. In general, the DFT-predicted $SF_{Ln/La}$ values greatly overestimate the actual $SF_{Ln/La}$ (e.g., DFT-predicted $SF_{Er/La} \approx 10^{10}$), but this is a well-known issue when computing SF among f-block elements.[16,25,68−70] Despite this overestimation, the qualitative trend across the series is accurately replicated. The lack of quantitative accuracy could stem from several sources, such as the level of theory used or the models not explicitly including solvent molecules. Alternate thermodynamic cycles, such as calculating the competition between 2 extractants as a $\Delta\Delta\Delta E_{La/Ln}$ as done with Eu/Am separation,[35,45] may further improve the cancellation of errors and bring results closer to chemical accuracy. Similarly, alternate schemes that can accommodate the impact of environmental factors in determining the SF can also improve predictive accuracy. Nevertheless, reliably identifying the selectivity trend is a crucial first step for rapid computational extractant screening and can direct whether a ligand is suitable for higher-level computational or experimental investigation as well as serving as a point of direct comparison to experimental results. As such, it is encouraging that our high-throughput workflow was able to (1) identify the proper extractant complex structures for different metals and (2) characterize the relative selectivity trend observed for the Ln series.

In addition to using the lowest energy structures, $\Delta\Delta E_{La/Ln}$ values were also computed using structures that were found within 5 kcal/mol of the most stable structure. For the early Ln's, there were no configurations ≤5.0 kcal/mol of the most stable structure (Figure 2B), so the distribution in $\Delta\Delta E_{La/Ln}$ shown in Figure 2C represents only the variance that arises from low-energy $Ln(NO_3)(H_2O)_{3(aq)}$ configurations. However, for Eu and later Ln's, up to seven alternative structures were

https://doi.org/10.1021/jacsau.4c00770
JACS Au 2025, 5, 631−641

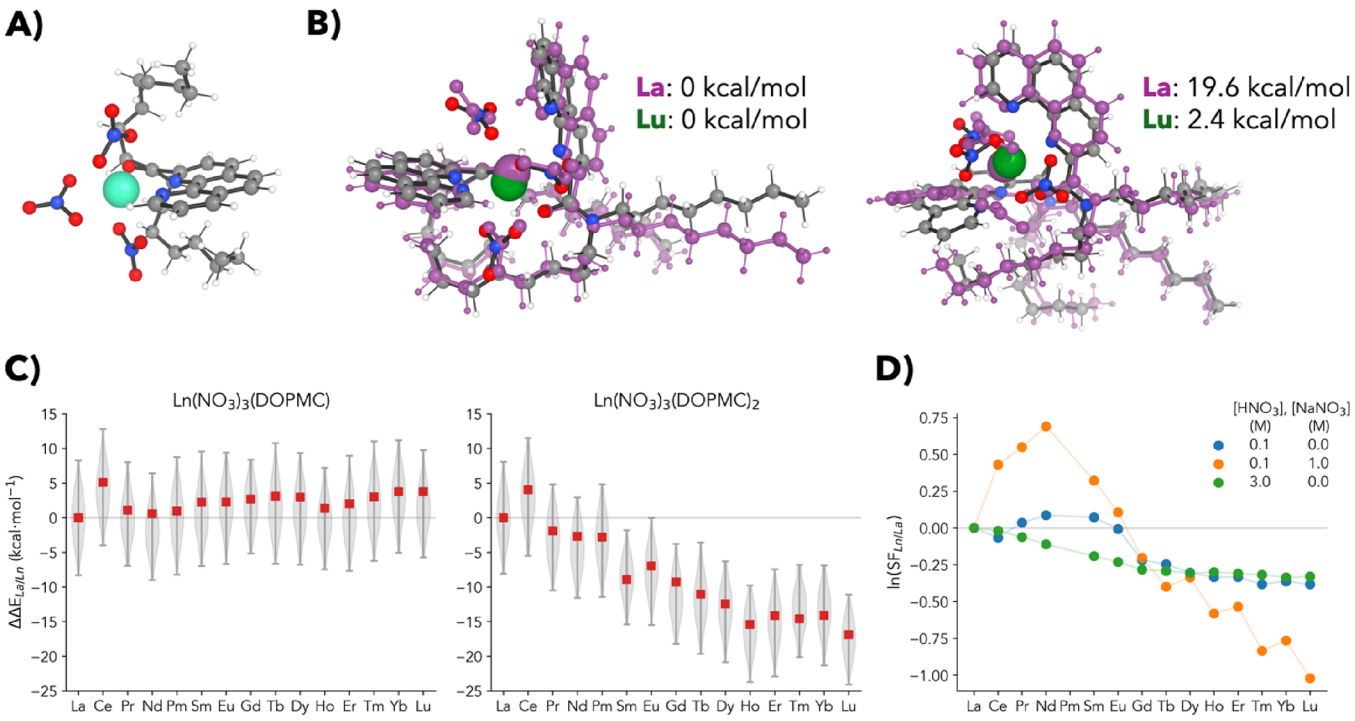

Figure 3. (A) Most stable $Ln^{III}(DOPMC)(NO_3)_3$ conformation identified. (B) Overlay and relative conformation energies for two $Ln^{III}(DOPMC)_2(NO_3)_3$ conformations for both La^{3+} (purple) and Lu^{3+}. (C) Predicted selectivities ($\Delta\Delta E_{La/Ln}$) for DOPMC using the lowest energy configuration (red) and structures ≤ 5 kcal/mol of the lowest energy configuration (gray) when either one two DOPMC ligands coordinate the Ln. (D) Experimental $\ln(SF_{Ln/La})$ for 7 ppm Ln^{3+} with 0.1 M DOPMC in varying acid and nitrate concentrations at 25 °C.[41]

identified within 5.0 kcal/mol, and therefore, the distribution of $\Delta\Delta E_{La/Ln}$ represents the variance that can arise from both low-energy $Ln(NO_3)(H_2O)_{3(aq)}$ and $Ln(18\text{-crown-6})(NO_3)_{3(org)}$ configurations. The ranges shown indicate two principal ideas: (1) the difference in $\Delta\Delta E_{La/Ln}$ that can arise from structures thermally accessible and (2) these ranges regularly overlap among neighboring Ln's, illustrating the potential for qualitative misinterpretation among relative selectivity if a less-robust structure search was performed beforehand. This further emphasizes the importance of a thorough sampling of the conformation space, as small differences in structure energies can impact $\Delta\Delta E_{La/Ln}$ selectivity predictions.

Ln(III)-DOPMC

Compared to the 18-crown-6 ligand, DOPMC presents a more challenging case for modeling complexes as more than one extractant ligand can bind to the Ln center, and the long carbon side chains increase configurational complexity. DOPMC (Figure 1) contains three potential coordinating atoms: the two nitrogen atoms of the phenanthroline and the oxygen atom of the amide. Both 1:1 and 1:2 ratio complexes containing three nitrates were explored with *Architector* using the same procedure as that for the 18-crown-6 ligand.

For the mono-DOPMC complex, *Architector* identified 10 distinct coordination structures. The primary variations were in the positioning of the nitrates relative to the phenanthroline plane and carbon bond rotations of the two octyl side chains (Figure S10). Upon DFT optimization, these 10 unique configurations spanned an energetic range of 18 kcal/mol. Contrary to the 18-crown-6 system, substituting the Gd center with other Ln ions resulted in no substantial change in the relative stability or structure (Figure S12) as the most stable configuration identified for the Gd complex (Figure 3A) remained the same across the series.

Conformer search for the bi-DOPMC complex identified four unique configurations where the two phenanthroline planes of the DOPMC ligands are positioned either perpendicular or parallel to each other (Figure S11). The most stable arrangement contained both DOPMC ligands coordinated with three bidentate nitrates, and two other configurations were within 5.0 kcal/mol of this structure. The lowest energy $Gd(DOPMC)_2$ complex was found to be the most stable structure across the Ln series (Figure 3B) up to Ho. For Ho−Yb, the first shell of two DOPMC ligands and three bidentate nitrates becomes overcrowded, and lower CN structures (CN = 10−11) containing one to two monodentate nitrates are favored. For Lu, the structure slightly rearranged during DFT relaxation, resulting in one DOPMC ligand becoming bidentate, with two and one bidentate and monodentate nitrates, respectively (Figure 3B). Similar to the 18-crown-6 ligand, there is a stark difference in the relative stability of certain configurations between the lightest and heaviest Ln's, where conformations that are 8−20 kcal/mol for $La(DOPMC)_2(NO_3)_3$ become <2.5 kcal/mol for Lu (Figure 3B and Figure S12). These observations spotlight the importance of configurational sampling among different Ln's to identify the lowest energy structures, as the stability for a given core configuration is sensitive to the Ln present.

Interestingly, the competitive complexation reaction for mono- and bi-DOPMC complexes yielded different predictions regarding the selectivity trends (Figure 3C). For the mono-DOPMC complex, there is little differentiation in computed $\Delta\Delta E_{La/Ln}$ among the different Ln's. Therefore, if this 1:1 structure was assumed to be the extracted species in the organic phase, the computed results would indicate poor

https://doi.org/10.1021/jacsau.4c00770
JACS Au 2025, 5, 631−641

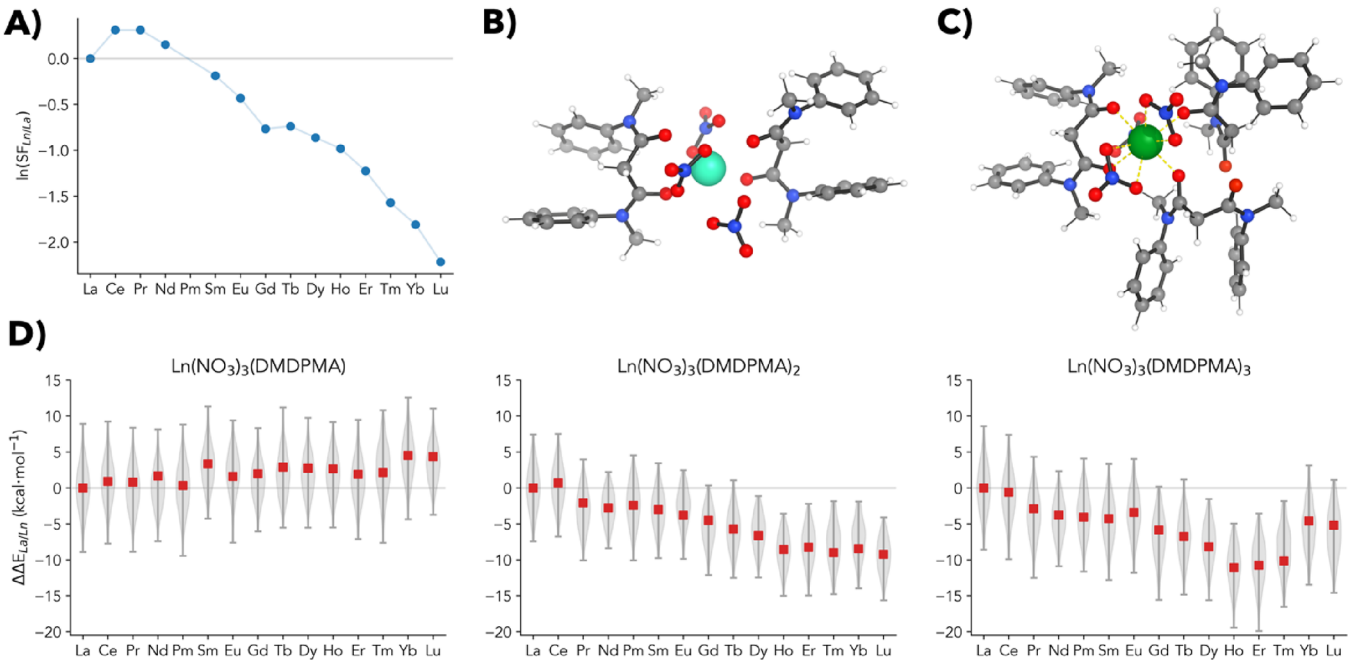

Figure 4. (A) Experimental $\ln(SF_{Ln/La})$ for 1 ppm Ln^{3+} with 0.2 M DMDPMA and 4 M HNO_3 at 23 °C.[43] (B) Most stable $Ln^{III}(DMDPMA)_2(NO_3)_3$ conformation shown with Gd. (C) Most stable $Lu^{III}(DMDPMA)_3(NO_3)_3$ conformation showing partial decomplexation of two DMDPMA ligands and suggesting oversaturation. (D) Predicted selectivities ($\Delta\Delta E_{La/Ln}$) for DMDPMA using the lowest energy configuration (red) and structures ≲5 kcal/mol of the lowest energy configuration (gray) when one to three DMDPMA ligands coordinate the Ln.

selectivity of the ligand for any of the Ln's, if not a slight preference for late Ln's over early Ln's. However, the predictions for bi-DOPMC show a definitive trend, with the $\Delta\Delta E_{La/Ln}$ value becoming more negative when transitioning to the heavier elements, with the exception of Ce predicted to be preferentially extracted over La.

Experimentally reported[41] separation factors for DOPMC are provided in Figure 3D and show an interesting case: while the early Ln's are preferentially extracted over later Ln's, depending on the concentration of acid and nitrates present, an increase in the selectivity among early Ln's is seen followed by a semiplateau around Nd and Sm. Though our predicted results for the 1:2 complex do capture the qualitative trend between early and late Ln's and predict greater selectivity for Ce over La, they do not show the continued increase and plateauing around Nd/Sm observed experimentally. This discrepancy likely arises from environmental factors affecting the system, as indicated by the sensitivity of SF to both acid and nitrate concentrations. These experimental variables can influence the involvement of nitrates in the first shell. Previous experimental and modeling studies on similar phenanthroline monoamide ligands[41,71−73] have proposed that Ln-(DOPMC)$_2$(NO$_3$)$_3$ complexes readily assemble for the early Ln ions, but as the ionic size decreases across the series, one of the nitrates transitions to the second shell to form [Ln-(DOPMC)$_2$(NO$_3$)$_2$]$^+$[NO$_3$]$^-$ complexes. Currently, our workflow is limited to sampling first shell structures and capturing trends that originate from the first shell chemistry. Expanding our workflow to explore both first- and second-sphere clusters may allow us to capture and quantify these secondary environmental effects.

Ln(III)-DMDPMA

The malonamide extractant, DMDPMA, coordinates the Ln^{3+} ion through its two amide oxygen atoms, allowing for the potential of 1:1, 1:2, and 1:3 complexes. Nine different Gd-complexes were identified for the mono- and bi-DMDPMA complexes, with four and two of these configurations within 5.0 kcal/mol of the most stable structure, respectively. Similar to the observations with DOMPC, the substitution of Gd with other Ln ions resulted in no substantial change in the relative stabilities and geometries of the configurations across the series for the mono-DMDPMA structures (Figure S16). For the bi-DMDPMA complexes, the relative energies among the three lowest configurations consistently remain <3 kcal/mol across the series. These low-lying Ln(DMDPMA)$_2$ complexes have all three nitrates coordinated bidentate until Lu(DMDPMA)$_2$, where two of the configurations rearrange to have one monodentate and two bidentate nitrates (CN = 9, Figure 4B).

For the tri-DMDPMA structures, 10 different Gd-complexes were identified with 4 of them within 5 kcal/mol of the lowest energy structure, while the total energy configuration spanned up to 15 kcal/mol. Interestingly, the lowest energy Gd-(DMDPMA)$_3$ structures do not have all three DMDPMA ligands fully coordinated with both oxygen atoms; instead, 1−2 DMDPMA ligands are monodentate. The lowest energy structure with all three of the DMDPMA ligand coordinated bidentates is 4.94 kcal/mol higher in energy but has one of the nitrates moved to the second shell. These structural rearrangements upon DFT optimization suggest an oversaturation of the first shell. This idea is reinforced when examining the metallovariants. When Gd is replaced with larger La and Ce, a structure containing three fully coordinated DMDPMA ligands (with 1 bidentate and 2 monodentate nitrates) is identified, but this structure remains ∼3 kcal/mol higher in energy than structures with DMDPMA not fully bound. For smaller Ln ions such as Yb and Lu, a configuration with two monodentate DMDPMAs and only two coordinated nitrates (CN = 8) becomes the most stable arrangement (Figure 4C), with the higher coordinated geometries significantly less stable

https://doi.org/10.1021/jacsau.4c00770
JACS Au 2025, 5, 631−641

(Figure S15). Altogether, overcrowding of the tri-DMDPMA structures indicates that a bi-DMDPMA first coordination shell (or possibly tri-DMDPMA structures with second sphere nitrates—structures not explored by our current workflow) is the most likely geometry.

Like the DOPMC complexes, different ligand ratios yield different predictions of trends in Ln selectivity for DMDPMA (Figure 4D). For the mono-DMDPMA complex, no notable selectivity trend is predicted across the Ln series, but the bi- and tri-DMDPMA complexes both predict preferential extraction of the early lanthanides over late lanthanides. An abrupt increase in selectivity for Yb and Lu is seen in the tri-DMDPMA complex, but the most stable complexes for both these elements are optimized to geometries with one of the nitrates in the second shell. Therefore, we expect this difference to be the cause of the break in the selectivity trend.

Reported experimental separation factors for DMDPMA[43] (Figure 4A) illustrate the early Ln's are preferentially extracted over later Ln's, with an initial increase and plateauing at Ce and Pr. Like the DOPMC system, our predicted results for the bi- and tri-DMDPMA capture the qualitative trend in selectivity across the series for this extractant. Neither ligand ratio captures the increased selectivity for Ce, Pr, and Nd over La, though, suggesting this selectivity originates from environmental effects beyond the core complex structure. While the exact Ln-DMDPMA extractant complex has not specifically been resolved experimentally, studies on other Ln-malonamide systems can give insight. Experimental and modeling studies have typically proposed the $Ln(DMDPMA)_2(NO_3)_3$ complex as the first coordination structure[74,75] and that the formation of both second sphere malonamides and supramolecular species can play significant roles in the extraction of Ln's into the organic phase.[76,77] Recently, solid-state complexes with the *N,N,N′,N′*-tetramethylmalonamide (TMMA) ligand have reported variation in the first shell composition (including $Ln(TMMA)_{N=1-3}$ complexes) and geometry (*cis*/*trans*-$TMMA_2$ spatial coordination) across the Ln series.[78] The diverse $Ln(DMDPMA)_{N=1-3}$ complexes reported in this work are comparable to the solid-state structures reported for $Ln(TMMA)_{N=1-3}$. Even though the solid-state structures may not be identical with the solution-state structures, those findings reiterate the importance of screening the configuration space of different Ln-ligand ratios to identify the proper Ln-extractant complex structure.

DISCUSSION

In this work, we utilized a unique, high-throughput computational approach for the *a priori* exploration of Ln-extractant structures, their configurational space, and the prediction of their liquid−liquid extraction selectivity trends. We first investigated a crown ether, confirming that the workflow could account for different ion/ligand positioning (inside and outside the ring) and nitrate denticity. In agreement with experimental evidence, the most stable conformation identified for the early and mid-Ln's contains the ion within the ring with bidentate nitrates on both planes of the ring. The smaller ionic radii of later Ln's led to conformations with the ion not fully bound by 18-crown-6 becoming more favorable and predicted that the $SF_{Ln/La}$ decreased from early to late Ln's. The Ln-extractant complexes for both a phenanthroline monocarboxamide and a malonamide ligand were subsequently explored to assess the impact of different Ln-ligand ratios and configurations on the predicted complex structure and SF. For both cases, 1:1 Ln-extractant complexes did not yield any distinct trends in Ln selectivity across the series. However, once additional extractant molecules coordinated the ion (1:2 or 1:3, depending on extractant and Ln identity), the $SF_{Ln/La}$ trend could be properly identified.

Two key guidelines emerged for the automated Ln-extractant structure screening done in this work. First, saturating the first coordination sphere with extractants is essential to obtaining general selectivity trends. This is demonstrated for the DOPMC and DMDPMA ligands, where the proper trend is not observed for the monoextractant models, but adding extractant molecules to form bi- and tri-ligand species captured the correct first shell chemistry and resulting trend. Second, it is critical to sample diverse first shell configurations instead of using only a single representative structure across the series. For all three ligands, the ranges of relative energies for the configurations spanned from 7 to 22 kcal/mol. Furthermore, while the lowest energy configuration for these three extractants was generally consistent among early and midlanthanides, the smaller size of the later Ln's, especially Yb and Lu, changed to favor different lower-coordination geometries. Traditional methods for designing structures can handle simple cases (such as the crown ether complex); however, high-throughput automated searches like the workflow detailed here allow us to accommodate the configurational complexity that arises from multiple Ln-extractant-counterion ratios in varying arrangements.

CONCLUSIONS

Developing novel extractants with improved selectivity for specific Ln's is central to advancing current solvent extraction systems, but this progress is hindered by the expensive resources and labor required to experimentally test diverse classes of ligands. Computational modeling can help initially screen candidate extractants, but traditional methods are limited in their ability to rapidly and accurately characterize new metal-extractant complexes. Ln selectivity is determined by small energy differences among Ln-extractant complexes, but the presence of multiple stable configurations can complicate predictions if local minimum structures are mistaken for the lowest energy structures.

Here, we applied a high-throughput computational workflow to automate the structural screening of three different Ln-extractant complexes, assess their configurational space, and predict their Ln selectivity trends. The findings highlight the necessity to include searches for both configurational and compositional structures to identify the lowest energy coordination complex and accurately predict selectivity trends. Furthermore, the lowest energy configuration identified for one Ln will not always be the same for other Ln's (especially for the later Ln's), so it is not necessarily appropriate to rely on a single configuration for computing Ln selectivity trends across the series.

While many physicochemical properties of Ln-extractant complexes are directly related to their core coordination structure, second shell extractants, anions, and solvent molecules still play a crucial role in dictating Ln-ligand structure and selectivity.[79−84] As such, upcoming improvements to *Architector* to automate the generation of a second shell of explicit molecules are underway. Finally, although this work focuses on lanthanide selectivity, the fundamental chemistries and importance of complex configuration sampling are broadly applicable to the exploration of any metal

https://doi.org/10.1021/jacsau.4c00770
JACS Au 2025, 5, 631−641

complexes. Thus, the methods and findings presented here represent a significant step toward a more robust, automated evaluation of novel metal−ligand complexes, which will benefit not only Ln extraction and separation techniques but metal-complex chemistries in general.

■ ASSOCIATED CONTENT

Supporting Information

The Supporting Information is available free of charge at https://pubs.acs.org/doi/10.1021/jacsau.4c00770.

Final structure coordinates and energies (ZIP)

Additional details on methodology testing and supporting figures (PDF)

■ AUTHOR INFORMATION

Corresponding Author

Ping Yang − *Theoretical Division, Los Alamos National Laboratory, Los Alamos, New Mexico 87545, United States;* orcid.org/0000-0003-4726-2860; Email: pyang@lanl.gov

Authors

Thomas J. Summers − *Theoretical Division, Los Alamos National Laboratory, Los Alamos, New Mexico 87545, United States;* orcid.org/0000-0002-4243-6078

Michael G. Taylor − *Theoretical Division, Los Alamos National Laboratory, Los Alamos, New Mexico 87545, United States*

Logan J. Augustine − *Theoretical Division, Los Alamos National Laboratory, Los Alamos, New Mexico 87545, United States;* orcid.org/0000-0002-0830-0820

Jan Janssen − *Theoretical Division, Los Alamos National Laboratory, Los Alamos, New Mexico 87545, United States;* Present Address: Max Planck Institute for Sustainable Materials, Max-Planck-Straße 1, 40237 Düsseldorf, Germany

Danny Perez − *Theoretical Division, Los Alamos National Laboratory, Los Alamos, New Mexico 87545, United States;* orcid.org/0000-0003-3028-5249

Enrique R. Batista − *Theoretical Division, Los Alamos National Laboratory, Los Alamos, New Mexico 87545, United States;* orcid.org/0000-0002-3074-4022

Complete contact information is available at: https://pubs.acs.org/10.1021/jacsau.4c00770

Author Contributions

CRediT: **Thomas Jeffrey Summers** data curation, formal analysis, visualization, writing - original draft; **Michael G. Taylor** software, validation, writing - review & editing; **Logan J. Augustine** data curation, validation, visualization, writing - review & editing; **Jan Janssen** software, writing - original draft; **Danny Perez** software, supervision, writing - original draft; **Enrique R. Batista** supervision, writing - review & editing; **Ping Yang** conceptualization, funding acquisition, project administration, resources, supervision, writing - review & editing.

Notes

The authors declare no competing financial interest.

■ ACKNOWLEDGMENTS

We gratefully acknowledge the support of the U.S. Department of Energy (DOE), Office of Science, Office of Basic Energy Sciences, Heavy Element Chemistry Program (KC0302031) under contract number E3M2 (T.J.S., M.G.T., D.P., E.R.B, P.Y.). L.J.A. acknowledges sponsored by the Glenn T. Seaborg Institute at LANL. J.J., P.Y., M.G.T., and D.P. are also grateful to the Institute for Pure and Applied Mathematics (IPAM) at UCLA for their hospitality during the program "New Mathematics for the Exascale", where the development of the high-throughput workflow was initiated. Los Alamos National Laboratory is operated by Triad National Security, LLC, for the National Nuclear Security Administration of the U.S. Department of Energy (contract no. 89233218CNA000001). This research used resources of the National Energy Research Scientific Computing Center (NERSC), a DOE Office of Science User Facility using NERSC award BES-ERCAP0023367 and BES-ERCAP0028946.

■ REFERENCES

(1) USGCRP *Fourth National Climate Assessment: Volume II Impacts, Risks, and Adaptation in the United States*; U.S. Global Change Research Program: Washington, DC, USA, 2018.

(2) Balaram, V. Rare Earth Elements: A Review of Applications, Occurrence, Exploration, Analysis, Recycling, and Environmental Impact. *Geosci. Front.* **2019**, *10* (4), 1285−1303.

(3) Cheng, S.; Li, W.; Han, Y.; Sun, Y.; Gao, P.; Zhang, X. Recent Process Developments in Beneficiation and Metallurgy of Rare Earths: A Review. *J. Rare Earths* **2024**, *42* (4), 629−642.

(4) Fujita, Y.; McCall, S. K.; Ginosar, D. Recycling Rare Earths: Perspectives and Recent Advances. *MRS Bull.* **2022**, *47* (3), 283−288.

(5) Leoncini, A.; Huskens, J.; Verboom, W. Ligands for F-Element Extraction Used in the Nuclear Fuel Cycle. *Chem. Soc. Rev.* **2017**, *46* (23), 7229−7273.

(6) Xie, F.; Zhang, T. A.; Dreisinger, D.; Doyle, F. A Critical Review on Solvent Extraction of Rare Earths from Aqueous Solutions. *Miner. Eng.* **2014**, *56*, 10−28.

(7) *DGA Resins Cartridge* | Eichrom Technologies Inc.; Eichrom Technologies, LLC: Lisle, IL, 2024. https://www.eichrom.com/products/dga-resins/

(8) Sato, T. Liquid-Liquid Extraction of Rare-Earth Elements from Aqueous Acid Solutions by Acid Organophosphorus Compounds. *Hydrometallurgy* **1989**, *22* (1), 121−140.

(9) Johnson, K. R.; Driscoll, D. M.; Damron, J. T.; Ivanov, A. S.; Jansone-Popova, S. Size Selective Ligand Tug of War Strategy to Separate Rare Earth Elements. *JACS Au* **2023**, *3* (2), 584−591.

(10) Stamberga, D.; Healy, M. R.; Bryantsev, V. S.; Albisser, C.; Karslyan, Y.; Reinhart, B.; Paulenova, A.; Foster, M.; Popovs, I.; Lyon, K.; Moyer, B. A.; Jansone-Popova, S. Structure Activity Relationship Approach toward the Improved Separation of Rare-Earth Elements Using Diglycolamides. *Inorg. Chem.* **2020**, *59* (23), 17620−17630.

(11) Vahidi, E.; Zhao, F. Environmental Life Cycle Assessment on the Separation of Rare Earth Oxides through Solvent Extraction. *J. Environ. Manage.* **2017**, *203*, 255−263.

(12) Sprecher, B.; Xiao, Y.; Walton, A.; Speight, J.; Harris, R.; Kleijn, R.; Visser, G.; Kramer, G. J. Life Cycle Inventory of the Production of Rare Earths and the Subsequent Production of NdFeB Rare Earth Permanent Magnets. *Environ. Sci. Technol.* **2014**, *48* (7), 3951−3958.

(13) Moyer, B. A.; Lumetta, G. J.; Bruffey, S. H.; Finkeldei, S.; Marsden, K. C.; Simpson, M. F.; Jensen, M. P.; Zalupski, P. R.; Clark, A. E.; Yang, P.; Horne, G. P. *Innovative Separations Research and Development Needs for Advanced Fuel Cycles*; ORNL/SPR-2022/2314; Oak Ridge National Laboratory: Oak Ridge, TN (United States), 2022. .

(14) Bünzli, J.-C. G. Benefiting from the Unique Properties of Lanthanide Ions. *Acc. Chem. Res.* **2006**, *39* (1), 53−61.
(15) Sasaki, Y.; Sugo, Y.; Morita, K.; Nash, K. L. The Effect of Alkyl Substituents on Actinide and Lanthanide Extraction by Diglycolamide Compounds. *Solvent Extr. Ion Exch.* **2015**, *33* (7), 625−641.
(16) Zhang, X.; Adelman, S. L.; Arko, B. T.; De Silva, C. R.; Su, J.; Kozimor, S. A.; Mocko, V.; Shafer, J. C.; Stein, B. W.; Schreckenbach, G.; Batista, E. R.; Yang, P. Advancing the Am Extractant Design through the Interplay among Planarity, Preorganization, and Substitution Effects. *Inorg. Chem.* **2022**, *61* (30), 11556−11570.
(17) An, L.; Yao, Y.; Hall, T. B.; Zhao, F.; Qi, L. Agile Synthesis and Automated, High-Throughput Evaluation of Diglycolamides for Liquid−Liquid Extraction of Rare-Earth Elements. *Green Chem.* **2024**, *26* (26), 7188−7197.
(18) Higgins, R. F.; Ruoff, K. P.; Kumar, A.; Schelter, E. J. Coordination Chemistry-Driven Approaches to Rare Earth Element Separations. *Acc. Chem. Res.* **2022**, *55* (18), 2616−2627.
(19) Li, S.; Jansone-Popova, S.; Jiang, D. Insights into Coordination and Ligand Trends of Lanthanide Complexes from the Cambridge Structural Database. *Sci. Rep.* **2024**, *14* (1), 11301.
(20) Sittel, T.; Meißner, M.; Keller, M.; Geist, A.; Panak, P. J. Spectroscopic Study on the Complexation of Trivalent Actinide and Lanthanide Ions with TEDGA in Solution. *Eur. J. Inorg. Chem.* **2024**, *27* (10), No. e202300720.
(21) Wang, X.; Peroutka, A. A.; Kravchuk, D. V.; Shafer, J. C.; Wilson, R. E.; Servis, M. J. Metadynamics Investigation of Lanthanide Solvation Free Energy Landscapes and Insights into Separations Energetics. *Chem. Sci.* **2024**, *15* (40), 16494−16502.
(22) Reddy, Th. D. N.; Ivanov, A. S.; Driscoll, D. M.; Jansone-Popova, S.; Jiang, D. Changes in Nitrate Binding with Lanthanides in BLPhen Complexes. *J. Mol. Liq.* **2023**, *387*, No. 122573.
(23) Massey, D.; Williams, C. D.; Mu, J.; Masters, A. J.; Motokawa, R.; Aoyagi, N.; Ueda, Y.; Antonio, M. R. Hierarchical Aggregation in a Complex Fluid—The Role of Isomeric Interconversion. *J. Phys. Chem. B* **2023**, *127* (9), 2052−2065.
(24) Ebenezer, C.; Solomon, R. V. Computational Tools and Techniques in Designing Ligands for the Selective Separation of Actinide and Lanthanide: A Review. *Comments Inorg. Chem.* **2024**, *44* (5), 385−459.
(25) Ivanov, A. S.; Bryantsev, V. S. A Computational Approach to Predicting Ligand Selectivity for the Size-Based Separation of Trivalent Lanthanides. *Eur. J. Inorg. Chem.* **2016**, *2016* (21), 3474−3479.
(26) Ustynyuk, Y. A.; Alyapyshev, M. Y.; Babain, V. A.; Ustynyuk, N. A. Quantum Chemical Modelling of Extraction Separation of Minor Actinides and Lanthanides: The State of the Art. *Russ. Chem. Rev.* **2016**, *85* (9), 917.
(27) O'Brien, R. D.; Summers, T. J.; Kaliakin, D. S.; Cantu, D. C. The Solution Structures and Relative Stability Constants of Lanthanide−EDTA Complexes Predicted from Computation. *Phys. Chem. Chem. Phys.* **2022**, *24* (17), 10263−10271.
(28) Summers, T. J.; Sobrinho, J. A.; de Bettencourt-Dias, A.; Kelly, S. D.; Fulton, J. L.; Cantu, D. C. Solution Structures of Europium Terpyridyl Complexes with Nitrate and Triflate Counterions in Acetonitrile. *Inorg. Chem.* **2023**, *62* (13), 5207−5218.
(29) Muller, J. M.; Berthon, C.; Couston, L.; Guillaumont, D.; Ellis, R. J.; Zorz, N.; Simonin, J.-P.; Berthon, L. Understanding the Synergistic Effect on Lanthanides(III) Solvent Extraction by Systems Combining a Malonamide and a Dialkyl Phosphoric Acid. *Hydrometallurgy* **2017**, *169*, 542−551.
(30) Yang, X.; Fang, D.; Chen, L.; Liu, Y.; Wang, S.; Xu, L.; Zhang, A.; Su, J.; Xu, C.; Xiao, C. Computation-Aided Development of Next-Generation Extractants for Trivalent Actinide and Lanthanide Separation. *JACS Au* **2024**.
(31) Cao, H.; Kang, Y.; Li, B.; Liu, Y.; Bao, M.; Li, H.; Zheng, Y.; Wang, L.; Weng, C.; Tang, X.; Wang, L.; Xu, C. Amine-Terminated Phenanthroline Diimides as Aqueous Masking Agents for Am(III)/Eu(III) Separation: An Alternative Ligand Design Strategy for Water-Soluble Lanthanide/Actinide Chelating Ligands. *Inorg. Chem.* **2024**, *63* (23), 10511−10518.
(32) Bursch, M.; Hansen, A.; Pracht, P.; Kohn, J. T.; Grimme, S. Theoretical Study on Conformational Energies of Transition Metal Complexes. *Phys. Chem. Chem. Phys.* **2021**, *23* (1), 287−299.
(33) Cotton, S. A.; Raithby, P. R. Systematics and Surprises in Lanthanide Coordination Chemistry. *Coord. Chem. Rev.* **2017**, *340*, 220−231.
(34) Moreau, J.; Guillon, E.; Pierrard, J.-C.; Rimbault, J.; Port, M.; Aplincourt, M. Complexing Mechanism of the Lanthanide Cations Eu3+, Gd3+, and Tb3+ with 1,4,7,10-Tetrakis(Carboxymethyl)-1,4,7,10-Tetraazacyclododecane (Dota)—Characterization of Three Successive Complexing Phases: Study of the Thermodynamic and Structural Properties of the Complexes by Potentiometry, Luminescence Spectroscopy, and EXAFS. *Chem. − Eur. J.* **2004**, *10* (20), 5218−5232.
(35) Clark, A. E.; Servis, M. J.; Liu, Z.; Martinez-Baez, E.; Su, J.; Batista, E. R.; Yang, P.; Wildman, A.; Stetina, T.; Li, X.; Newcomb, K.; Maginn, E. J.; Autschbach, J.; Dixon, D. A. Solvent Extraction through the Lens of Advanced Modeling and Simulation. In *Ion Exchange and Solvent Extraction*; CRC Press, 2019.
(36) Balcells, D.; Drudis-Solé, G.; Besora, M.; Dölker, N.; Ujaque, G.; Maseras, F.; Lledós, A. Some Critical Issues in the Application of Quantum Mechanics/Molecular Mechanics Methods to the Study of Transition Metal Complexes. *Faraday Discuss.* **2003**, *124* (0), 429−441.
(37) Vitek, A. K.; Jugovic, T. M. E.; Zimmerman, P. M. Revealing the Strong Relationships between Ligand Conformers and Activation Barriers: A Case Study of Bisphosphine Reductive Elimination. *ACS Catal.* **2020**, *10* (13), 7136−7145.
(38) Besora, M.; Braga, A. A. C.; Ujaque, G.; Maseras, F.; Lledós, A. The Importance of Conformational Search: A Test Case on the Catalytic Cycle of the Suzuki−Miyaura Cross-Coupling. *Theor. Chem. Acc.* **2011**, *128* (4), 639−646.
(39) Taylor, M. G.; Burrill, D. J.; Janssen, J.; Batista, E. R.; Perez, D.; Yang, P. Architector for High-Throughput Cross-Periodic Table 3D Complex Building. *Nat. Commun.* **2023**, *14* (1), 2786.
(40) Janssen, J.; Surendralal, S.; Lysogorskiy, Y.; Todorova, M.; Hickel, T.; Drautz, R.; Neugebauer, J. Pyiron: An Integrated Development Environment for Computational Materials Science. *Comput. Mater. Sci.* **2019**, *163*, 24−36.
(41) Simonnet, M.; Kobayashi, T.; Shimojo, K.; Yokoyama, K.; Yaita, T. Study on Phenanthroline Carboxamide for Lanthanide Separation: Influence of Amide Substituents. *Inorg. Chem.* **2021**, *60* (17), 13409−13418.
(42) Riahi, F.; Bagherzade, M. Separation of Some Lanthanide (III) Ions by using 18-Crowns-6 Derivatives from Acidic Solution. *J. Appl. Sci.* **2010**, *10* (16), 1781−1786.
(43) Narita, H.; Yaita, T.; Tamura, K.; Tachimori, S. Study on the Extraction of Trivalent Lanthanide Ions with N,N′-Dimethyl-N,N′-Diphenyl-Malonamide and Diglycolamide. *J. Radioanal. Nucl. Chem.* **1999**, *239* (2), 381−384.
(44) Clark, A. E.; Yang, P.; Shafer, J. C. Coordination of Actinides and the Chemistry Behind Solvent Extraction. *Exp. Theor. Approaches Actinide Chem.* **2018**, 237−282.
(45) Keith, J. M.; Batista, E. R. Theoretical Examination of the Thermodynamic Factors in the Selective Extraction of Am3+ from Eu3+ by Dithiophosphinic Acids. *Inorg. Chem.* **2012**, *51* (1), 13−15.
(46) Ali, S. M.; Pahan, S.; Bhattacharyya, A.; Mohapatra, P. K. Complexation Thermodynamics of Diglycolamide with F-Elements: Solvent Extraction and Density Functional Theory Analysis. *Phys. Chem. Chem. Phys.* **2016**, *18* (14), 9816−9828.
(47) Yang, Y.; Liu, J.; Yang, L.; Li, K.; Zhang, H.; Luo, S.; Rao, L. Probing the Difference in Covalence by Enthalpy Measurements: A New Heterocyclic N-Donor Ligand for Actinide/Lanthanide Separation. *Dalton Trans.* **2015**, *44* (19), 8959−8970.
(48) Lehman-Andino, I.; Su, J.; Papathanasiou, K. E.; Eaton, T. M.; Jian, J.; Dan, D.; Albrecht-Schmitt, T. E.; Dares, C. J.; Batista, E. R.; Yang, P.; Gibson, J. K.; Kavallieratos, K. Soft-Donor Dipicolinamide

https://doi.org/10.1021/jacsau.4c00770
JACS Au 2025, 5, 631−641

Derivatives for Selective Actinide(III)/Lanthanide(III) Separation: The Role of S- vs. O-Donor Sites. *Chem. Commun.* **2019**, *55* (17), 2441−2444.
(49) Bannwarth, C.; Ehlert, S.; Grimme, S. GFN2-xTB—An Accurate and Broadly Parametrized Self-Consistent Tight-Binding Quantum Chemical Method with Multipole Electrostatics and Density-Dependent Dispersion Contributions. *J. Chem. Theory Comput.* **2019**, *15* (3), 1652−1671.
(50) Bannwarth, C.; Caldeweyher, E.; Ehlert, S.; Hansen, A.; Pracht, P.; Seibert, J.; Spicher, S.; Grimme, S. Extended Tight-Binding Quantum Chemistry Methods. *WIREs Comput. Mol. Sci.* **2021**, *11* (2), No. e1493.
(51) te Velde, G.; Bickelhaupt, F. M.; Baerends, E. J.; Fonseca Guerra, C.; van Gisbergen, S. J. A.; Snijders, J. G.; Ziegler, T. Chemistry with ADF. *J. Comput. Chem.* **2001**, *22* (9), 931−967.
(52) van Lenthe, E.; Ehlers, A.; Baerends, E.-J. Geometry Optimizations in the Zero Order Regular Approximation for Relativistic Effects. *J. Chem. Phys.* **1999**, *110* (18), 8943−8953.
(53) Caldeweyher, E.; Ehlert, S.; Hansen, A.; Neugebauer, H.; Spicher, S.; Bannwarth, C.; Grimme, S. A Generally Applicable Atomic-Charge Dependent London Dispersion Correction. *J. Chem. Phys.* **2019**, *150* (15), 154122.
(54) Klamt, A.; Schüürmann, G. COSMO: A New Approach to Dielectric Screening in Solvents with Explicit Expressions for the Screening Energy and Its Gradient. *J. Chem. Soc. Perkin Trans. 2* **1993**, *5*, 799−805.
(55) Klamt, A. Conductor-like Screening Model for Real Solvents: A New Approach to the Quantitative Calculation of Solvation Phenomena. *J. Phys. Chem.* **1995**, *99* (7), 2224−2235.
(56) Marenich, A. V.; Cramer, C. J.; Truhlar, D. G. Generalized Born Solvation Model SM12. *J. Chem. Theory Comput.* **2013**, *9* (1), 609−620.
(57) Peeples, C. A.; Schreckenbach, G. Implementation of the SM12 Solvation Model into ADF and Comparison with COSMO. *J. Chem. Theory Comput.* **2016**, *12* (8), 4033−4041.
(58) Ahn, D. H.; Bass, N.; Chu, A.; Garlick, J.; Grondona, M.; Herbein, S.; Ingólfsson, H. I.; Koning, J.; Patki, T.; Scogland, T. R. W.; Springmeyer, B.; Taufer, M. Flux: Overcoming Scheduling Challenges for Exascale Workflows. *Future Gener. Comput. Syst.* **2020**, *110*, 202−213.
(59) Bombieri, G.; de Paoli, G.; Benetollo, F.; Cassol, A. Crown Ether Complexes of Lanthanoid and Actinoid Elements. Crystal and Molecular Structure of Nd(NO3)3 (18-Crown-6). *J. Inorg. Nucl. Chem.* **1980**, *42* (10), 1417−1422.
(60) Bünzli, J.-C. G.; Klein, B.; Wessner, D. Crystal and Molecular Structure of the 1:1 Complex of 18-Crown-6 Ether with Neodymium Nitrate. *Inorg. Chim. Acta* **1980**, *44*, L147−L149.
(61) Rogers, R. D.; Rollins, A. N. Primary to Secondary Sphere Coordination of 15-Crown-5 to Lanthanide(III) Chlorides: Structural Analysis of [MCl3(15-Crown-5)] (M = La, Ce) and [Er(OH2)8]Cl3·15-Crown-5. *J. Chem. Crystallogr.* **1994**, *24* (8), 531−537.
(62) Backer-Dirks, J. D. J.; Cooke, J. E.; Galas, A. M. R.; Ghotra, J. S.; Gray, C. J.; Hart, F. A.; Hursthouse, M. B. Complexes of Lanthanide Ions with the Crown Ether 1,4,7,10,13,16-Hexaoxacyclo-Octadecane. *J. Chem. Soc., Dalton Trans.* **1980**, *11*, 2191−2198.
(63) Bünzli, J.-C. G.; Klein, B.; Wessner, D.; J. Schenk, K.; Chapuis, G.; Bombieri, G.; De Paoli, G. Crystal and Molecular Structure of the 4:3 Complex of 18-Crown-6 Ether with Neodymium Nitrate. *Inorg. Chim. Acta* **1981**, *54*, L43−L46.
(64) Jinzhong, Z.; Xi, W.; Dexi, W. The Stability of Coordination Compounds of Some Crown Ethers with Lanthanide(III) Ions. *Inorg. Chim. Acta* **1984**, *94* (1), 41−43.
(65) Izatt, R. M.; Lamb, J. D.; Christensen, J. J.; Haymore, B. L. Anomalous Stability Sequence of Lanthanide(III) Chloride Complexes with 18-Crown-6 in Methanol. Abrupt Decrease to Zero from Gadolinium(3+) Ion to Terbium(3+) Ion. *J. Am. Chem. Soc.* **1977**, *99* (25), 8344−8346.
(66) Bünzli, J.-C. G.; Klein, B.; Wessner, D.; Alcock, N. W. Crystal Structure and Emission Spectrum of Tris(Nitrato)-1,4,7,10-Tetraoxacyclododecane-Europium(III). *Inorg. Chim. Acta* **1982**, *59*, 269−274.
(67) Nash, K. L. Chapter 121 Separation Chemistry for Lanthanides and Trivalent Actinides. *Handb. Phys. Chem. Rare Earths* **1994**, *18*, 197−238.
(68) Kelley, M. P.; Bessen, N. P.; Su, J.; Urban, M.; Sinkov, S. I.; Lumetta, G. J.; Batista, E. R.; Yang, P.; Shafer, J. C. Revisiting Complexation Thermodynamics of Transplutonium Elements up to Einsteinium. *Chem. Commun.* **2018**, *54* (75), 10578−10581.
(69) Healy, M. R.; Ivanov, A. S.; Karslyan, Y.; Bryantsev, V. S.; Moyer, B. A.; Jansone-Popova, S. Efficient Separation of Light Lanthanides(III) by Using Bis-Lactam Phenanthroline Ligands. *Chem. − Eur. J.* **2019**, *25* (25), 6326−6331.
(70) Sadhu, B.; Dolg, M. Enhancing Actinide(III) over Lanthanide(III) Selectivity through Hard-by-Soft Donor Substitution: Exploitation and Implication of Near-Degeneracy-Driven Covalency. *Inorg. Chem.* **2019**, *58* (15), 9738−9748.
(71) Nakase, M.; Kobayashi, T.; Shiwaku, H.; Suzuki, S.; Grimes, T. S.; Mincher, B. J.; Yaita, T. Relationship Between Structure and Coordination Strength of N and N,O-Hybrid Donor Ligands with Trivalent Lanthanides. *Solvent Extr. Ion Exch.* **2018**, *36* (7), 633−646.
(72) Simonnet, M.; Suzuki, S.; Miyazaki, Y.; Kobayashi, T.; Yokoyama, K.; Yaita, T. Lanthanide Intra-Series Separation by a 1,10-Phenanthroline Derivative: Counterion Effect. *Solvent Extr. Ion Exch.* **2020**, *38* (4), 430−440.
(73) Sun, M.; Xu, L.; Yang, X.; Wang, S.; Lei, L.; Xiao, C. Complexation Behaviors of a Tridentate Phenanthroline Carboxamide Ligand with Trivalent F-Block Elements in Different Anion Systems: A Thermodynamic and Crystallographic Perspective. *Inorg. Chem.* **2022**, *61* (6), 2824−2834.
(74) Iveson, P. B.; Drew, M. G. B.; Hudson, M. J.; Madic, C. Structural Studies of Lanthanide Complexes with New Hydrophobic Malonamide Solvent Extraction Agents†. *J. Chem. Soc., Dalton Trans.* **1999**, *20*, 3605−3610.
(75) Parks, B. W.; Gilbertson, R. D.; Hutchison, J. E.; Healey, E. R.; Weakley, T. J. R.; Rapko, B. M.; Hay, B. P.; Sinkov, S. I.; Broker, G. A.; Rogers, R. D. Solution and Structural Investigations of Ligand Preorganization in Trivalent Lanthanide Complexes of Bicyclic Malonamides. *Inorg. Chem.* **2006**, *45* (4), 1498−1507.
(76) Ellis, R. J.; D'Amico, L.; Chiarizia, R.; Antonio, M. R. Solvent Extraction of Cerium(III) Using an Aliphatic Malonamide: The Role of Acid in Organic Phase Behaviors. *Sep. Sci. Technol.* **2012**, *47* (14−15), 2007−2014.
(77) Ellis, R. J.; Antonio, M. R. Coordination Structures and Supramolecular Architectures in a Cerium(III)−Malonamide Solvent Extraction System. *Langmuir* **2012**, *28* (14), 5987−5998.
(78) Kravchuk, D. V.; Wang, X.; Servis, M. J.; Wilson, R. E. Structural Trends and Vibrational Analysis of N,N,N′,N′−Tetramethylmalonamide Complexes Across the Lanthanide Series. *Eur. J. Inorg. Chem.* **2024**, *27* (6), No. e202300632.
(79) O'Connell-Danes, J. G.; Ngwenya, B. T.; Morrison, C. A.; Love, J. B. Selective Separation of Light Rare-Earth Elements by Supramolecular Encapsulation and Precipitation. *Nat. Commun.* **2022**, *13* (1), 4497.
(80) de Bettencourt-Dias, A.; Beeler, R. M.; Zimmerman, J. R. Anion-π and H-Bonding Interactions Supporting Encapsulation of [Ln(NO3)6/5]3−/2− (Ln = Nd, Er) with a Triazine-Based Ligand. *J. Am. Chem. Soc.* **2019**, *141* (38), 15102−15110.
(81) Baldwin, A. G.; Ivanov, A. S.; Williams, N. J.; Ellis, R. J.; Moyer, B. A.; Bryantsev, V. S.; Shafer, J. C. Outer-Sphere Water Clusters Tune the Lanthanide Selectivity of Diglycolamides. *ACS Cent. Sci.* **2018**, *4* (6), 739−747.
(82) Brigham, D. M.; Ivanov, A. S.; Moyer, B. A.; Delmau, L. H.; Bryantsev, V. S.; Ellis, R. J. Trefoil-Shaped Outer-Sphere Ion Clusters Mediate Lanthanide(III) Ion Transport with Diglycolamide Ligands. *J. Am. Chem. Soc.* **2017**, *139* (48), 17350−17358.
(83) de Bettencourt-Dias, A.; Beeler, R. M.; Zimmerman, J. R. Secondary-Sphere Chlorolanthanide(III) Complexes with a 1,3,5-

https://doi.org/10.1021/jacsau.4c00770
JACS Au 2025, 5, 631−641

Triazine-Based Ligand Supported by Anion−π, π−π, and Hydrogen-Bonding Interactions. *Inorg. Chem.* **2020**, *59* (1), 151−160.
(84) Olejniczak, M.; Vallet, V.; Gomes, A. S. P. Modeling Environment Effect on Heavy-Element Compounds. In *Comprehensive Computational Chemistry* (First Edition); Yáñez, M., Boyd, R. J., Eds.; Elsevier: Oxford, 2024; pp 129−154. .

https://doi.org/10.1021/jacsau.4c00770
JACS Au 2025, 5, 631−641